TISSUE ENGINEERING: Part A
Volume 16, Number 7, 2010

DOI: 10.1089/ten.tea.2009.0602

Decellularized Rhesus Monkey Kidney as a Three-Dimensional Scaffold for Renal Tissue Engineering

Karina H. Nakayama, B.S.,[1] Cynthia A. Batchelder, Ph.D.,[1]
Chang I. Lee, Ph.D.,[1] and Alice F. Tarantal, Ph.D.[1,2]

The goal of this study was the production of a decellularized kidney scaffold with structural, mechanical, and physiological properties necessary for engineering basic renal structures *in vitro*. Fetal, infant, juvenile, and adult rhesus monkey kidney sections were treated with either 1% (v/v) sodium dodecyl sulfate or Triton X-100 followed by quantitative and qualitative analysis. Comparison of decellularization agents and incubation temperatures demonstrated sodium dodecyl sulfate at 4°C to be most effective in preserving the native architecture. Hematoxylin and eosin staining confirmed the removal of cellular material, and immunohistochemistry demonstrated preservation of native expression patterns of extracellular matrix proteins, including heparan sulfate proteoglycan, fibronectin, collagen types I and IV, and laminin. Biomechanical testing revealed a decrease in the compressive modulus of decellularized compared to fresh kidneys. Layering of fetal kidney explants on age-matched decellularized kidney scaffolds demonstrated the capacity of the scaffold to support Pax2+/vimentin+ cell attachment and migration to recellularize the scaffold. These findings demonstrate that decellularized kidney sections retain critical structural and functional properties necessary for use as a three-dimensional scaffold and promote cellular repopulation. Further, this study provides the initial steps in developing new regenerative medicine strategies for renal tissue engineering and repair.

Introduction

In 2008 the Scientific Registry for Transplant Recipients reported approximately 5,800 living donor kidney transplant recipients and over 78,600 patients remaining on the waitlist at the end of the survey year. Although the transplant rate among waitlisted patients was 20%, about 7% of patients died before receiving a kidney transplant.[1] Children under the age of 18 made up 2.8% of new patients added to the waitlist. Alternative methods for patients waiting for whole-organ transplants are desperately needed. A solution to ease transplant demands is the application of tissue engineering that could be used to develop functional tissue replacements.

A primary challenge in tissue engineering is the production of tissues with the functional complexity required for transplantation. One tissue engineering strategy is the use of natural acellular tissue matrices as three-dimensional biomaterial scaffolds to facilitate the formation of new tissues by potentiating cell–cell interactions. Decellularized tissue matrices are the remaining extracellular matrix (ECM) of tissues treated to remove cells, while preserving the composition, mechanical integrity, and biological activity of the ECM. The process of decellularization can be accomplished with chemical treatments, such as sodium dodecyl sulfate (SDS) or Triton X-100, which are detergents that disrupt cell membranes as well as cell–cell and cell–ECM bonds.[2] Several decellularized tissue and organ matrices have been successfully applied in clinical and preclinical studies, including dermis,[3,4] small intestinal submucosa,[5] heart valves,[6,7] bladder,[8] and heart.[9] In addition, ligament,[10] nerve,[11] amniotic membrane,[12] vocal fold lamina propria,[13] esophagus,[14] trachea,[15,16] and liver[17] have been studied for their tissue engineering potential as decellularized scaffolds.

Decellularized tissues are ideal natural scaffolds due to the preservation of native ECM architecture as well as cell–ECM binding domains critical in promoting cell attachment, migration, and proliferation. To date, no studies have examined sections of decellularized kidney as potential scaffolds for renal tissue engineering and in a clinically relevant rhesus

[1]Center of Excellence in Translational Human Stem Cell Research, California National Primate Research Center and [2]Departments of Pediatrics and Cell Biology and Human Anatomy, University of California, Davis, California.

monkey model. The goal of the current study was to examine the physical and biological properties of decellularized rhesus monkey kidney during ontogeny and changes with maturation and aging, as well as the potential use as a three-dimensional scaffold for engineering basic renal structures *in vitro*. The primary hypothesis explored was that decellularized kidneys possess functional ECM proteins and the ability to provide the framework for recellularization *in vitro*. This was addressed by decellularizing kidney sections across age groups (fetal, infant, juvenile, and adult) and subsequent quantitative and qualitative analysis of the decellularized kidney scaffold and its propensity for recellularization using explants from unrelated donors.

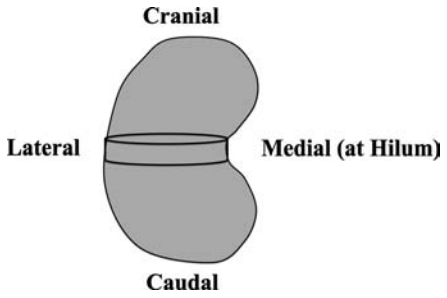

FIG. 1. Orientation of transverse section from kidneys of different age groups (fetal, infant, juvenile, and adult).

Materials and Methods

Tissue collection

All animal protocols were approved before implementation by the Institutional Animal Care and Use Committee at the University of California, Davis, and all procedures conformed to the requirements of the Animal Welfare Act. Activities related to animal care were performed in accordance with standard operating procedures at the California National Primate Research Center (CNPRC). Tissue harvests were performed using established methods and protocols.[18] Kidney transverse sections were collected from fetal (second and third trimester), infant (newborns to 1 year postnatal age), juvenile (1–3 years postnatal age), and adult (4–12 years of age) rhesus monkeys (*Macaca mulatta*; $n = 34$). All tissues were placed in Dulbecco's modified Eagle's medium (Invitrogen, Carlsbad, CA) upon collection and until processing, which was accomplished at the time of harvest. All experiments were performed under sterile conditions.

Decellularization

Kidney sections were washed twice with phosphate-buffered saline (PBS; Invitrogen) followed by a decellularization solution of either 1% (v/v) SDS (Invitrogen) or 1% (v/v) Triton X-100 (Sigma, St. Louis, MO) diluted in distilled water at either 4°C or 37°C. Decellularization solution was changed 8 h after initial tissue harvest and then every 48 h until tissues were transparent (7–10 days). Decellularized kidney scaffolds were gently washed with PBS, and cryo-embedded in optimum cutting temperature compound (Sakura Finetek/Tissue Tek, Torrance, CA), or fixed in 10% phosphate-buffered formalin (Thermo Fisher Scientific, Waltham, MA) and embedded in paraffin, or stored in 10% (v/v) penicillin/streptomycin (Invitrogen) in PBS at 4°C until use. Specimens from juveniles and adults were used for initial determination of decellularization strategies and were photographed fresh and after 4 and 10 days of treatment.

Rate of decellularization

Decellularization rates of fetal, infant, juvenile, and adult kidney sections were determined by starting weight (mg) or volume (mm^3) divided by the duration (days) of treatment necessary to achieve decellularization. Measurements of each of the transverse sections collected were recorded (longest diameter measured from medial [hilum] to lateral [outer border of the cortex], shortest diameter, and section thickness) with calipers (see Fig. 1), and the volume was calculated (assumed to be an elliptical cylinder). Rates of decellularization were grouped according to age (fetal, infant, juvenile, or adult), and a mean rate was calculated for each age group. The fold-change in volume of tissues decellularized with different treatments was calculated as final volume/initial volume.

Histology and immunofluorescence

Fresh, SDS-decellularized, and Triton X-100–decellularized paraffin-embedded and cryo-embedded kidneys were sectioned (5 μm), and morphology was analyzed with hematoxylin and eosin (H&E) staining and for detection of cell nuclei, with immunohistochemistry for ECM proteins (see below). The protocol for frozen-section immunohistochemistry was described by Leapley *et al.*[19] Briefly, sections were soaked in PBS for 5 min before fixing in cold methanol for 10 min at ≤ -20°C. Slides were blocked with 2% goat serum (Sigma) in blocking buffer (1% bovine serum albumin [BSA] in PBS) for 20 min at room temperature. After washing twice with PBS, slides were incubated with primary antibody diluted in blocking buffer overnight in a humidified chamber at 4°C. The primary antibodies to heparan sulfate proteoglycan (clone 7E12; Millipore, Billerica, MA) diluted 1:10, fibronectin (clone P1H11; Chemicon International, Temecula, CA) diluted 1:200, collagen type I (clone COL-1; Sigma) diluted 1:1000, collagen type IV (clone COL-94; Thermo Fisher Scientific) diluted 1:1000, and laminin (clone A5; Thermo Fisher Scientific) diluted 1:25 were used. Mouse immunoglobulin G1 (IgG1; Dako, Carpinteria, CA) and rat IgG2a (Abcam, Cambridge, MA) were used for isotype controls. Slides were washed twice for 5 min with PBS and then incubated with secondary antibody dilutions for 1 h in the dark at room temperature. Secondary antibodies used were Alexa Fluor 488 goat anti-mouse (Invitrogen) and Alexa Fluor 594 goat anti-rat (Invitrogen) diluted 1:200 in blocking buffer. Slides were washed twice with PBS before mounting with one drop of ProLong® Gold antifade reagent with 4′,6-diamidino-2-phenylindole (Invitrogen), and then a coverslip was placed. Slides were stored at ≤ -20°C until photomicrographs were taken with an Olympus microscope (Olympus, Center Valley, PA) and images were recorded with Olympus soft image viewer.

Biomechanical testing

Fresh adult ($n = 2$) and juvenile ($n = 1$) kidney sections were cut into cylinders 8 mm in diameter and 5 mm in

thickness with an 8 mm biopsy punch (Med Plus, Monsey, NY) in triplicate. Specimens were analyzed using an Instron 3345 materials testing machine (Instron, Norwood, MA) before and after undergoing decellularization for 7 days. A preload of 0.25 N was applied to samples and the modulus (Young's compressive stress 0–0.10 mm/mm) was obtained from the first 10% of the linear graph of the compressive load versus extension curve.

Recellularization

Before recellularization, stored scaffolds were soaked overnight in sterile filtered (0.8 μm pore size; Millipore) 70% (v/v) ethanol in super-Q water and rehydrated in 10% penicillin/streptomycin in PBS for 24 h at 4°C. Late second/early third-trimester fetal kidney explants ($n = 3$) were layered on an age-matched unrelated decellularized kidney scaffold and cultured in explant medium (500 mL Dulbecco's modified Eagle's medium/F12 [Invitrogen], 25 ng/mL prostaglandin E (PGE) [Sigma], 1% insulin/transferrin/selenium [Sigma], 10% fetal bovine serum [Invitrogen], and 1% penicillin/streptomycin) for 5 days. Preliminary studies with fetal kidney explants quantified expression of apoptotic genes by polymerase chain reaction and determined a culture period of 5 days to be efficient without evidence of apoptosis. Therefore, after 5 days in culture, layered explants were either cryo-embedded in optimum cutting temperature compound or fixed in 10% formalin, embedded in paraffin, and stained with H&E, or immunohistochemistry was performed as described below. Photomicrographs were taken using an Olympus microscope.

Immunofluorescence

Immunohistochemistry was performed on paraffin-embedded sections of the layered explant for cytoskeletal and renal-specific proteins. The protocol for paraffin sections was described by Batchelder *et al.*[20] Briefly, sections were rehydrated in xylene followed by graded concentrations of ethanol. Slides were washed in PBS before heat-mediated antigen retrieval in citrate buffer (pH 6; Invitrogen) was performed. After cooling, decreasing concentrations of warm citrate buffer was applied to each slide followed by Background Sniper (BioCare Medical, Concord, CA) for 20 min. Slides were washed twice with PBS followed by incubation for 1 h with blocking buffer (1% BSA, 0.1% fish skin gelatin, 0.1% Triton X, and 0.05% Tween-20) with 2% goat serum. After two washes with PBS, primary antibody diluted in primary antibody buffer (1% BSA and 0.1% fish skin gel) was incubated with slides overnight in a humidified chamber at 4°C. Primary antibodies used were paired box gene 2 (*Pax2*, polyclonal; Invitrogen) diluted 1:100, Wilms tumor 1 (WT1, clone 6F-H2; Invitrogen) diluted 1:100, wide spectrum cytokeratin (polyclonal; Abcam) diluted 1:50, and vimentin (clone V6389; Sigma) diluted 1:100. Mouse IgG1 (Dako), and rabbit IgG (Invitrogen) isotype controls were used. Slides were washed with PBS for 5 min and incubated with secondary antibody for 1 h in the dark at room temperature. Secondary antibodies used were Alexa Fluor 488 goat anti-mouse (Invitrogen) and Alexa Fluor 594 goat anti-rabbit (Invitrogen) diluted 1:200 in fluorescence antibody diluent (BioCare Medical). After washing twice with PBS, slides were mounted with ProLong Gold antifade reagent with 4′,6-diamidino-2-phenylindole, and a coverslip was placed.

Statistics

The results were analyzed by Student's two-tailed *t*-test. A *p*-value of <0.05 was assessed as significant. All data are shown as mean ± standard error of the mean.

Results

Optimization of decellularization parameters

The first goal of the study was to determine which decellularization treatment produced tissue scaffolds with complete removal of cellular material, minimal changes in tissue volume, and well-preserved ECM. Comparison of decellularization solutions and incubation temperatures demonstrated a solution of 1% SDS incubated at 4°C to be most effective in preserving the native ECM architecture (Fig. 2). At the higher incubation temperature of 37°C, extensive changes in gross morphology of the tissues were observed, with a visual decrease in tissue volume with SDS treatment. At the lower incubation temperature of 4°C, the tissues experienced minimal changes in morphology.

After 10 days of decellularization, H&E-stained sections confirmed gross observations (Fig. 3). Qualitative analysis of tissues decellularized with SDS at 4°C revealed well-preserved architecture and demonstrated the absence of cell nuclei, confirming removal of intact cells. The ECM comprising the glomerular basement membrane and tubules remained intact, and the collagen matrix of surrounding epithelium and connective tissue was tightly organized. Decellularization with SDS at 37°C was associated with an increase in ECM compaction and disruption of ECM basement membrane (Fig. 3H, M). Triton X-100 decellularization at both temperatures resulted in disruption of basement membrane and demonstrated a loss of glomerular ECM organization, an increase in Bowman's space, and incomplete decellularization (Fig. 3N, O). Cell debris occupied empty spaces within the tissue. Cell nuclei were noted in the renal pelvis and glomeruli with 4°C Triton X-100–decellularized tissues (Fig. 3I) and within all renal structures throughout the tissue when processed at 37°C (Fig. 3J).

A change in tissue volume was recorded as a function of decellularization. Tissue measurements were taken before and after treatment. Values are reported in cubic millimeters for volume, and the fold-change was calculated as the final decellularized tissue measurements divided by the original fresh tissue measurements. A value close to 1 represents little change in tissue volume, whereas values significantly greater or less than 1 represent large changes in tissue volume. Decellularization with SDS at 4°C and Triton X-100 at 4°C resulted in minimal changes in tissue volume, and both decellularization strategies had a small fold change in volume of 0.94 ± 0.10. Decellularization with SDS at 37°C resulted in a significant loss of volume with a fold-change of 0.47 ± 0.10. A significant difference in volume fold-change was observed (0.94 ± 0.10 vs. 0.47 ± 0.10, $p < 0.05$) when tissues decellularized with SDS at 4°C were compared to those decellularized at 37°C. These observations suggest that decellularization at 37°C is detrimental to ECM tissue composition. It was determined that optimal decellularization occurred at an incubation temperature of 4°C, which induced a more mild and gradual decellularization. On the basis of

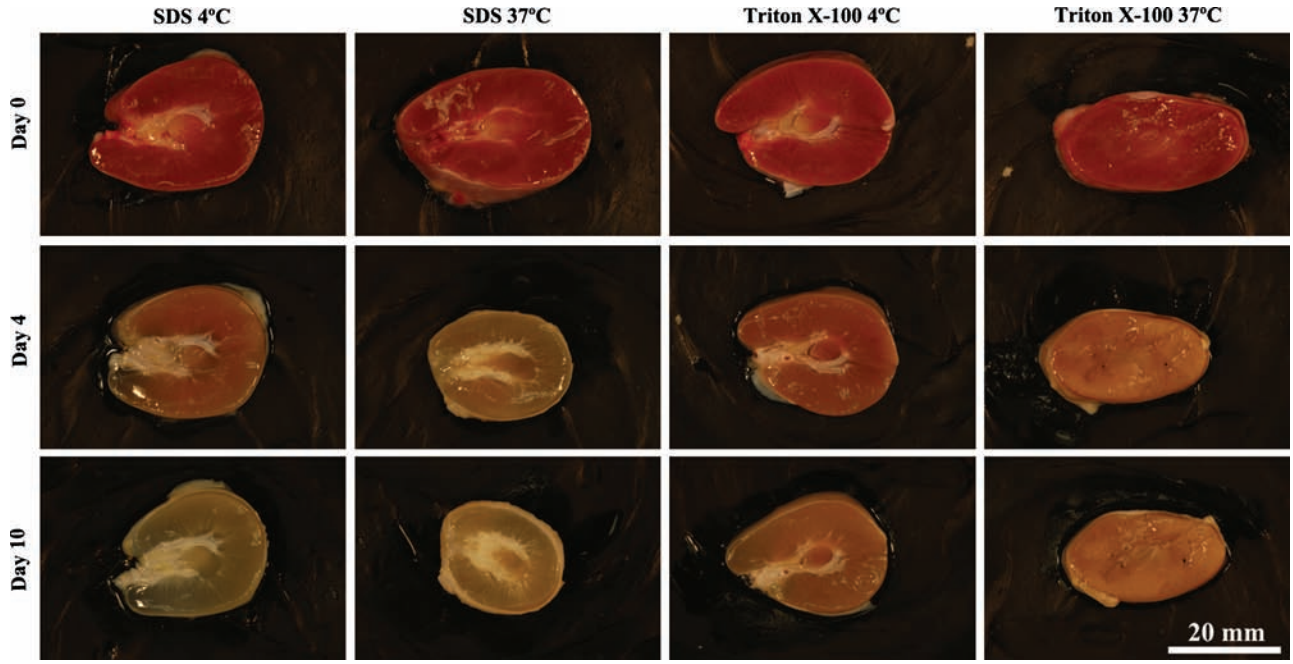

FIG. 2. Decellularization of juvenile rhesus monkey kidney transverse sections. Kidney sections were incubated with a decellularization solution of 1% SDS or 1% Triton X-100 at either 4°C or 37°C for 10 days. Images of the same section were taken on days 0, 4, and 10 of the decellularization process. SDS, sodium dodecyl sulfate. Color images available online at www.liebertonline.com/ten.

these findings, all further decellularization was performed at an incubation temperature of 4°C, and as described below.

Immunofluorescence of ECM proteins

Immunohistochemistry demonstrated expression of common ECM proteins, including heparan sulfate proteoglycan, fibronectin, collagen types I and IV, and laminin (Fig. 4). All five of these proteins displayed expression patterns in decellularized tissue similar to native tissue. Localization of collagen type I and IV was observed in the tubules and Bowman's capsule, with a distinct absence of collagen type I from the glomerular basement membrane (Fig. 4C, I, O). A double stain of collagen type IV and laminin demonstrated

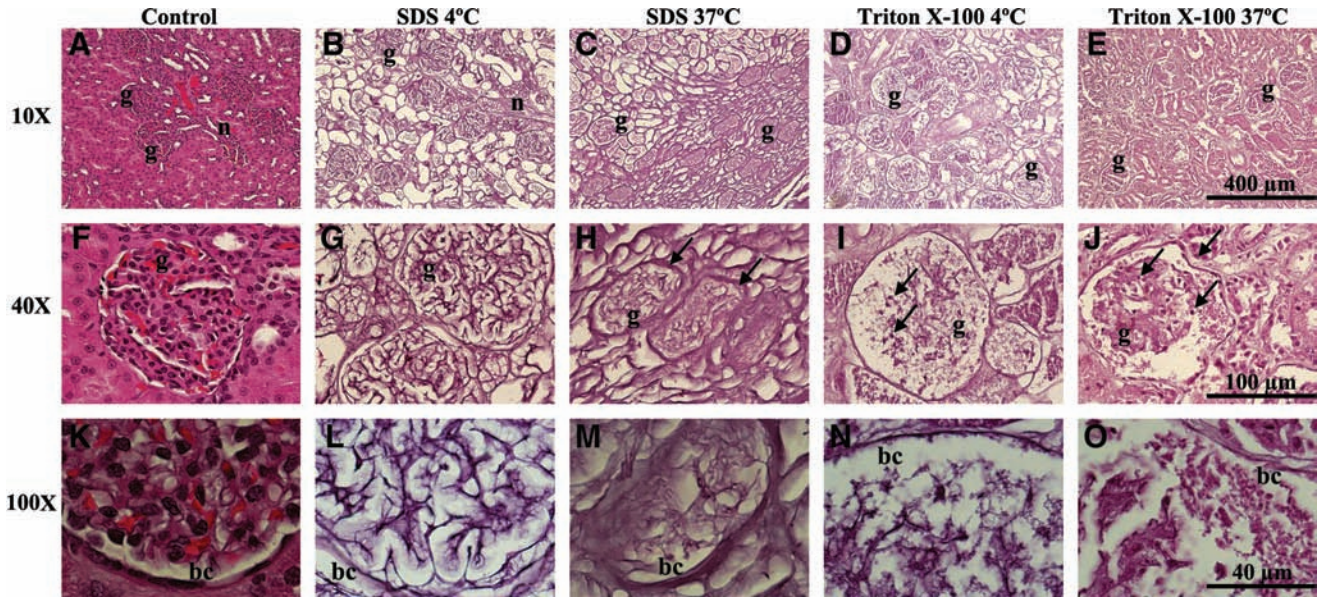

FIG. 3. Morphology. H&E stain of control (**A, F, K**) and decellularized adult rhesus monkey kidney sections. H&E of kidney decellularized with 1% SDS at 4°C (**B, G, L**) or 37°C (**C, H, M**), or 1% Triton X-100 at 4°C (**D, I, N**) or 37°C (**E, J, O**) for 10 days. Structurally intact glomerular basement membrane remained after decellularization with SDS at 4°C (**L**). Condensed ECM resulting from treatment with SDS at 37°C (**H, M,** arrows), and severe disruption of basement membrane from treatment with Triton X-100 (**I, N,** arrows); note residual cell nuclei (**J, O,** arrows). H&E, hematoxylin and eosin; ECM, extracellular matrix; g, glomeruli; bc, Bowman's capsule. Color images available online at www.liebertonline.com/ten.

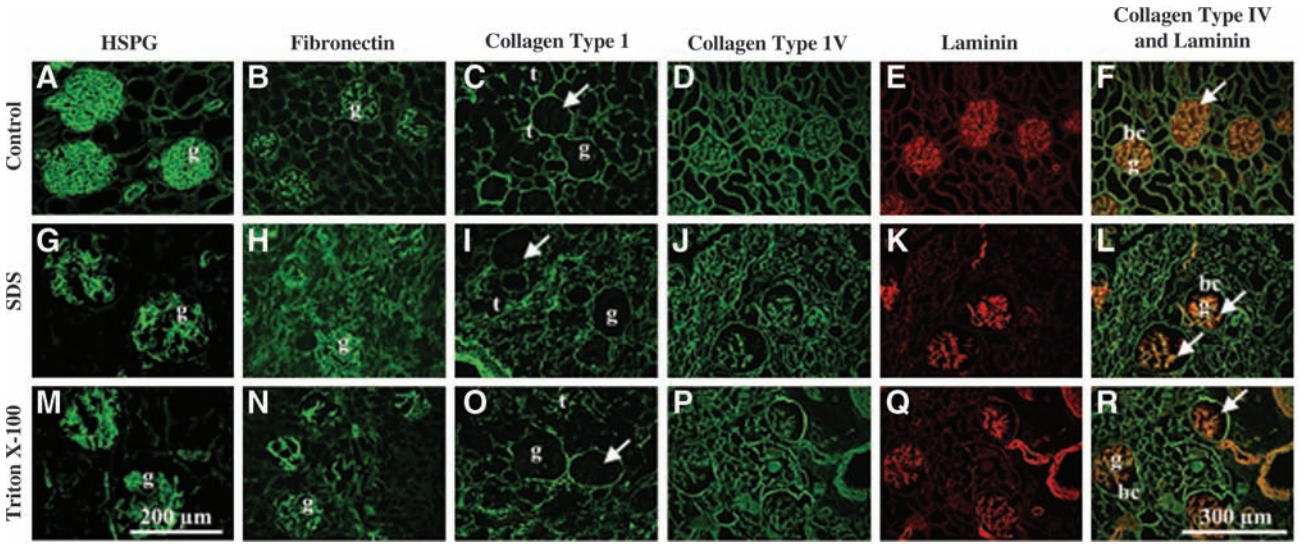

FIG. 4. Immunohistochemistry of control and decellularized kidney. Staining of ECM proteins in adult kidney sections (**A–F**), and after decellularization in 1% SDS (**G–L**) or 1% Triton X-100 (**M–R**) (20×). Decellularized tissues display the same localization of ECM proteins to glomeruli (g), tubules (t), and Bowman's capsule (bc) as control (no decellularization). Absence of collagen type I (**C, I, O,** arrows) and expression of HSPG (**A, G, M**) and fibronectin (**B, H, N**) in the glomerular basement membrane noted. Retention of distinct glomerular basement membrane (**F, L, R,** arrows) composition with co-localization of collagen type IV and laminin was more pronounced in SDS-decellularized tissue compared to Triton X-100. HSPG, heparan sulfate proteoglycan.

characteristic co-localization of these proteins to the glomerular basement membrane after decellularization with either SDS or Triton X-100 (Fig. 4F, L, R). In summary, although treatment with Triton X-100 and SDS at 4°C produced well-preserved ECM proteins, only the latter generated scaffolds resulting in minimal changes in volume and with no evidence of cell nuclei. On the basis of these findings, it was determined that a decellularization solution of 1% SDS was optimal and all further decellularization was performed with 1% SDS as the primary decellularization solution. This protocol is represented in the data presented, below.

Decellularization rate

Kidney sections were decellularized with 1% SDS at 4°C until complete decellularization had been qualitatively identified by tissue transparency. Mean volumetric and weight decellularization rates were calculated in mm^3/day or mg/day. It was found that kidney sections decellularized at an age-dependent volumetric rate. Adult kidneys decellularized at the fastest rate, followed by juvenile, and then infant, with fetal kidneys decellularizing at the slowest rate (Table 1). Decellularization based on starting tissue weight demonstrated similar age dependence with a more rapid rate of decellularization corresponding to the most mature tissues. Formation of a thin viscous capsule was observed surrounding fetal tissues within the first 24 h of decellularization as well as an increase in viscosity of the decellularization solution in which tissues were incubated, suggesting increased retention of water and salts close to the tissue due to greater presence of polysaccharide chains in fetal ECM.

Table 1. Mean Weight and Volumetric Decellularization Rate

Age group (n)	*Weight decellularization rate (mg/day)*	*Volumetric decellularization rate (mm^3/day)*
Fetal (7)	38 ± 6	18 ± 3
Infant (4)	113 ± 7^{a}	80 ± 6^{a}
Juvenile (3)	148 ± 15^{a}	103 ± 11^{a}
Adult (5)	$187 \pm 23^{a,b}$	$167 \pm 21^{a–c}$

Values represent mean ± standard error of the mean.
[a]Significant difference from fetal values, as determined by a two-tailed *t*-test ($p < 0.01$).
[b]Significant difference from infant values, as determined by a two-tailed *t*-test ($p < 0.05$).
[c]Significant difference from juvenile values, as determined by a two-tailed *t*-test ($p < 0.05$).

Biomechanical testing

Biomechanical testing was conducted with juvenile and adult kidney sections and revealed a decrease in the compressive modulus of decellularized specimens compared to fresh nondecellularized kidneys ($n = 3$), corresponding to a decrease in stiffness, a measure of resistance to deformation, of decellularized scaffolds (Fig. 5). A sample graph of the compressive load versus extension of cylindrical biopsies from one kidney before and after decellularization is shown (Fig. 5A). The slope, designated by linear lines that are tangent to and extrapolated from the first 10% of the linear portion of the compression curve, is the compressive modulus and was averaged among three test samples for each specimen. Fresh tissue samples were compressed until failure; however, decellularized tissues did not undergo failure within the tested compression range. A smaller modulus results from a larger deformation for a given applied load and indicates decreased stiffness, and a larger modulus

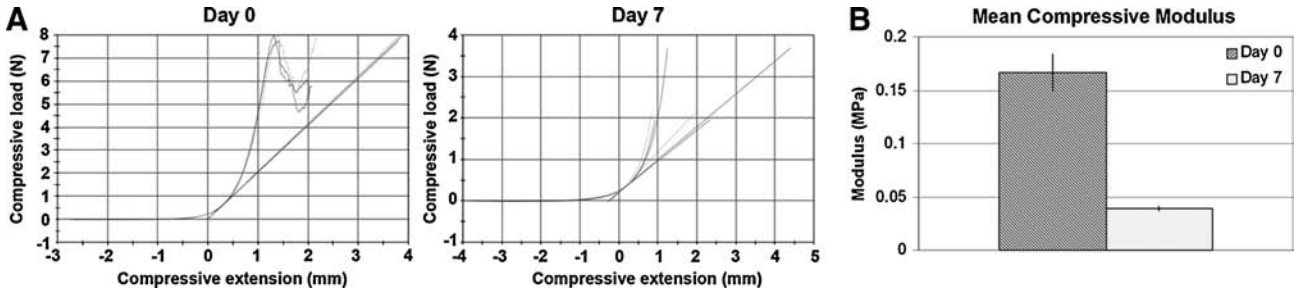

FIG. 5. Biomechanical testing. Graph of compressive load versus extension before decellularization on day 0 and after complete decellularization on day 7 for one specimen. The slope (compressive modulus) is designated by linear lines tangent to the curve (**A**). Young's compressive modulus was calculated from the first 10% of the linear section of the compression curve for each specimen. Graph of the mean compressive modulus and corresponding standard error of the mean for day 0 and day 7 kidney is shown in megapascals (MPa) (**B**).

indicates increased stiffness. Remaining kidney ECM after decellularization demonstrated a decrease in compressive modulus, suggesting that the specimen was less stiff or softer compared to controls (Fig. 5B). Slight compaction of ECM resulting from the decellularization process and loss of fluid-filled cellular material are likely responsible for the observed decrease in the compressive modulus.

Recellularization

Late second/early third trimester fetal kidney explants ($n = 3$) were layered on age-matched unrelated donor decellularized kidney scaffolds and cultured for 5 days. After 3 days in culture, the explants had fused with the scaffolds. H&E staining revealed migration of cells from the explant into the scaffold up to a depth of approximately 300 μm for the maximum of 5 days in culture evaluated (Fig. 6). Migration was localized to the explant/scaffold border as well as to the outer margins of the scaffold in contact with culture medium. No cells were evident within the bulk volume of the scaffold. Immunohistochemistry for the mesenchymal marker vimentin and epithelial marker cytokeratin, as well as the renal marker Pax2 and the transcription factor WT1, common to developing renal vesicles, was used to identify the specific phenotype of cells migrating from the explant to the scaffold by comparison with fresh and explant kidneys. Vimentin is typically located in the cytosol and is removed by SDS decellularization. Immunohistochemical staining confirmed removal of vimentin from the decellularized kidney scaffold (Fig. 7). The absence of vimentin staining within SDS-decellularized scaffolds suggests removal of intracellular and cytoskeletal materials and contrasted with strong staining in the explant, which enabled observation of a distinct explant/scaffold border and easy identification of cell migration beyond the explant boundary. Cells within the scaffold presented two distinct phenotypes, either as dense cell clusters positive for both vimentin and cytokeratin, or as individual vimentin-positive/cytokeratin-negative cells. These same two cell populations appeared to be positive for Pax2 with a few cells also positive for WT1. Fresh fetal kidney and kidney maintained in explant culture for 5 days weakly double-stained for vimentin and cytokeratin in some ureteric buds (Fig. 7). Vimentin-positive cells near the scaffold/explant border were oriented toward the scaffold and elongated in morphology, suggesting active migration into the scaffold.

Discussion

Twenty-six million Americans have chronic kidney disease with progression of the disease leading to kidney failure and the need for a kidney transplant to sustain life.[21] Approximately one-third of pediatric kidney-related illnesses are due to disruption of normal kidney development, resulting in abnormalities such as aplasia, dysplasia, and obstructive uropathy.[22] Current treatments such as dialysis offer temporary solutions for patients as they wait for a replacement organ; however, sustainable treatments are necessary to effectively address the problem of transplant organ supply and rejection.

Approaches to kidney tissue engineering have investigated the use of renal progenitors and precursors in three-dimensional niches to generate specific renal structures, such as renal tubules and glomeruli.[23,24] The complex interactions that occur during kidney development provide both framework and recipe for engineering renal tissue. The formation of the definitive kidney (metanephros) is the result of tightly regulated and highly organized reciprocal molecular interactions between the metanephric blastema (future excretory component) and the ureteric bud (future collecting system). Signals from the blastema induce branching morphogenesis of the ureteric bud and drive mesenchymal cells surrounding the bud tips to form renal vesicles that transition into epithelial comma-shaped and then S-shaped bodies to eventually become the glomeruli. Endothelial cells infiltrate the epithelium during the S-shaped stage to form the capillaries of the glomerular tuft and lead to the maturation of the glomerular basement membrane, which is composed of ECM components, including laminin, collagen IV, entactin/nidogen, proteoglycans, and fibronectin.[25–27]

During development of the definitive kidney, ECM is a morphogenic modulator responsible for mediating cellular organization, regulating signal transduction pathways, and controlling cell growth and proliferation. The composition, expression pattern, and concentration of ECM macromolecules are specific to a given developmental time frame. Well-orchestrated interactions with other macromolecules and cells present during this stage of development facilitate normal nephrogenesis.[28] Recapitulation of kidney ontogeny by reproducing the developmental niche with the appropriate ECM and cell populations will provide the best opportunity for the same interactions to occur *in vitro*. Therefore, this study investigated the use of nature's scaffold, decel-

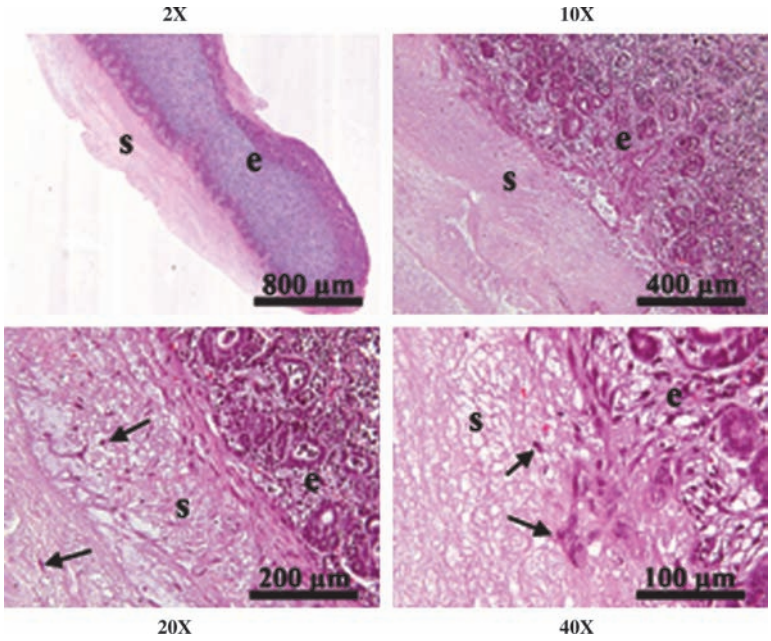

FIG. 6. Layered decellularized kidney scaffold and kidney explant. Fetal kidney explant was layered on an age-matched decellularized kidney scaffold and cultured for 5 days. H&E-stained sections of the explant/scaffold reveal migration of cells (arrows) from the explant (e) into the decellularized scaffold (s).

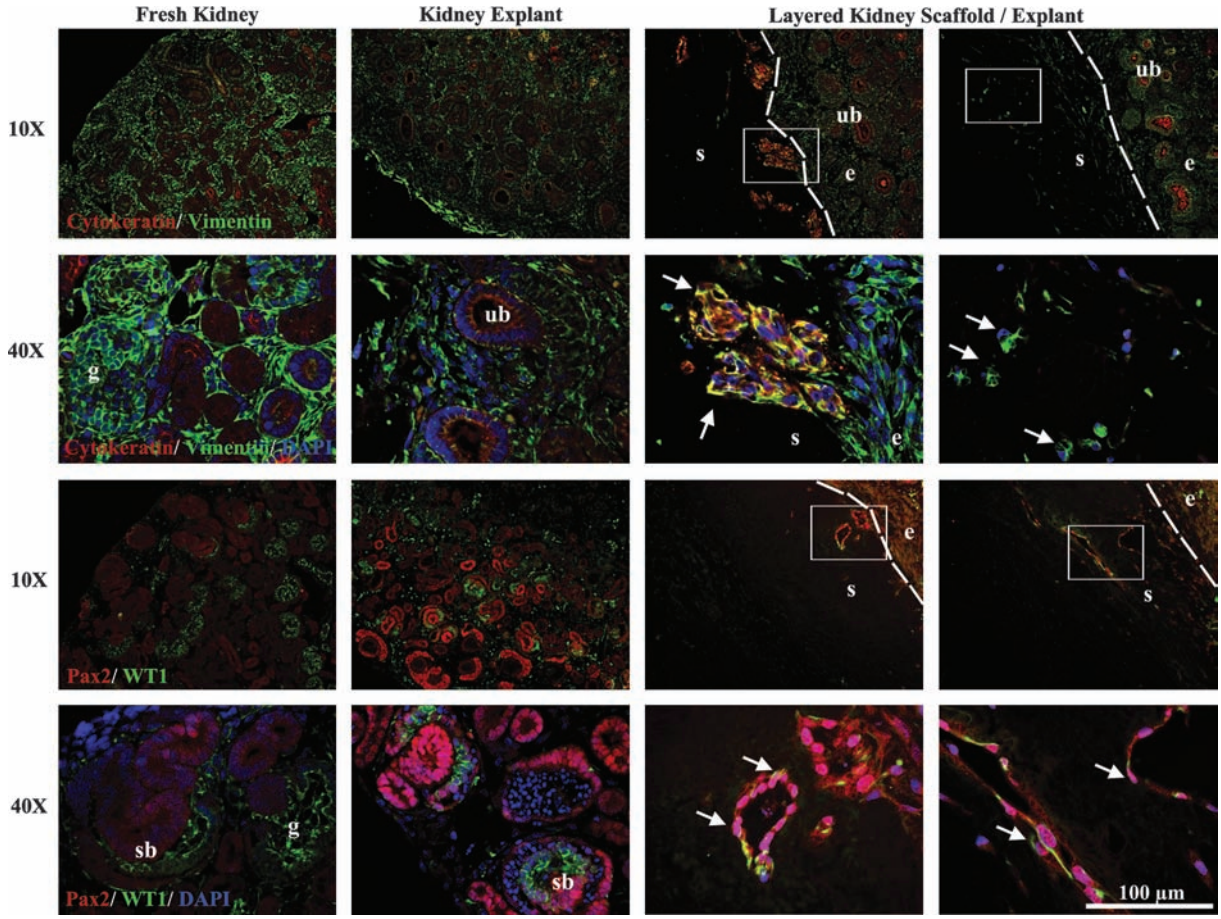

FIG. 7. Immunohistochemical staining of layered kidney scaffold and explant. Fresh and explant-cultured kidneys were stained for cytokeratin/vimentin or Pax2/WT1 for reference and renal structures—glomerulus (g), ureteric bud (ub), and S-shaped body (sb) are noted. Dotted line denotes boundary between scaffold (s) and explant (e). The rectangle in the 10× image highlights the region magnified in the 40× image. The nephrogenic zone of the explant is shown in direct contact with the scaffold, and arrows highlight populations of nucleated cells that have migrated into the scaffold cortex. DAPI, 4′,6-diamidino-2-phenylindole.

lularized kidney sections, to serve as a biologically active blueprint and modulator of renal recellularization and tissue engineering. Unlike most reports of applied decellularized tissues, age-related differences in decellularization were examined. The current study has demonstrated that decellularized rhesus monkey kidneys of all ages possess well-preserved histoarchitecture and functional ECM proteins, and that fetal kidneys as tested maintain the ability to support cell attachment and migration.

The goal of this study was to develop a decellularized kidney scaffold conducive to cellular repopulation for renal tissue engineering and determine whether there are unique differences depending on age. Because this is the first study to examine decellularization of nonhuman primate kidney tissue sections, optimization of decellularization treatment was required and extensive characterization of the scaffold's physical and biomechanical properties was needed to provide insight for scaffold recellularization. Detergents such as Triton X-100 and SDS are commonly used to decellularize tissues. There is still debate over which agent achieves optimal decellularization. Results from this study demonstrated that SDS was the most effective for decellularization of kidney sections. Triton X-100 was unable to completely decellularize the tissues and caused greater disruption of the basement membrane and connective tissue ECM. A study by Cartmell and Dunn[29] reported greater cell removal by SDS compared to Triton X-100 and showed that rat tendon treated with Triton X-100 resulted in the disruption of tendon collagen structure, whereas disruption was not seen in SDS-treated tendon.[29] In contrast, Woods and Gratzer[30] reported increased collagen denaturation of SDS-treated ligament and decreased glycosaminoglycan content. However, immunohistochemical analysis revealed only SDS treatment resulted in complete removal of the intracellular cytoskeletal protein, vimentin, compared with Triton X-100 or the organic solvent, tributyl phosphate. These studies suggest decellularization agent's effectiveness and destabilization of ECM are tissue specific. To ensure selection of optimal decellularization treatment for kidney sections, four treatment conditions were evaluated and a solution of 1% SDS at 4°C was most effective based on the following criteria: (1) minimal changes in tissue volume, (2) complete removal of cellular nuclei, and (3) preservation of functional ECM epitopes. With this treatment anuclear kidney scaffolds were produced that enabled moderate infiltration of cells from a fresh tissue explant. To our knowledge, this is the first study to examine decellularization of kidney tissue sections and in a clinically relevant nonhuman primate model.[31–33] The close phylogenetic relationship and shared developmental and anatomical features of this model provide translational relevance and unique insights into future applications for regenerative medicine.

Fetal kidneys from the late second trimester are in the process of undergoing active nephrogenesis, during which time the constant remodeling of the developing kidney and presence of primitive cell types may potentiate differential susceptibility of tissue to SDS compared to more mature tissues. During nephrogenesis, induction of the metanephric mesenchyme is followed by the loss of the ECM proteins, collagen types I and III, and fibronectin, and the formation of cell aggregates and mesenchyme condensates.[34] Removal of these cells and condensates with SDS treatment may leave large spaces devoid of ECM in the nephrogenic zone, resulting in collapse of the scaffold and prevention of further decellularization of the innermost cells. As the size of the nephrogenic zone decreases with increasing postnatal age, the condensing mesenchyme is replaced with mature renal structures and ECM. In older tissues, the microstructure of the scaffold experiences minimal collapse, which likely is responsible for allowing diffusion of SDS into the tissue for faster decellularization and may account for the observed increase in decellularization rate with advancing age. The current study has demonstrated age-dependent decellularization behavior of kidney sections, suggesting that critical differences in cell and ECM composition are important considerations for age-specific renal tissue engineering. These findings will aid in understanding potential age-related differences when scaffolds of different ages are decellularized and recellularized.

Biomechanical testing of engineered scaffolds and cellularized constructs is a common assessment of preservation of functional integrity and scaffold characterization.[35] Unfortunately, decellularization of tissues has been associated with changes in biomechanical properties. Increased tensile stiffness was noted in decellularized ligament[36] and a decrease in mechanical strength (burst pressure) for esophagus acellular matrix tissue.[37] Ott *et al.*[9] reported higher tangential modulus of decellularized heart compared to cadaveric rat ventricles; however, this group was able to successfully recellularize the matrix, suggesting that slight changes in biomechanical properties do not necessarily hinder cellular repopulation. In the study described herein, the compressive modulus of decellularized juvenile and adult kidneys decreased when compared to fresh tissue. Although biomechanical integrity is not a primary measure of functional ability for decellularized kidney scaffolds compared to engineered load bearing tissues, alteration of biomechanical properties of decellularized kidney may influence behavior of cells during repopulation; future biomechanical tests will need to be conducted after scaffold recellularization to assess how changes in the mechanical properties impact cellular repopulation.

To establish the feasibility of using a layered explant/scaffold culture for recellularization, decellularized fetal kidney scaffolds were cultured with age-matched fresh kidney explants from unrelated donors. Studies in which cell populations were seeded on SDS-decellularized tissues have demonstrated variable success in cellular repopulation. Reluctance of cells to infiltrate SDS-treated tissue was observed by Brown *et al.*[38] as well as studies published by Cartmell and Dunn[39] for patellar tendon. In contrast, Ott *et al.*[9] demonstrated successful recellularization of SDS-decellularized rat hearts with cardiomyocytes. These studies suggest that SDS decellularization does not necessarily prevent recellularization and is likely dependent on tissue type, the decellularization protocol, and cells used for repopulation. Histological analysis of the layered explant/scaffolds in the study described here revealed that the scaffolds were capable of supporting cell attachment and migration. Select locations in which developing cortical renal structures, such as ureteric buds and renal vesicles, were in direct contact with the scaffold showed migration of Pax2-positive cells with two distinct phenotypes. The first phenotype of dispersed, individual cells double-positive for vimentin and Pax2 is likely of

mesenchymal origin. The second phenotype of cell clusters triple-positive for vimentin, cytokeratin, and Pax2 may originate from the ureteric bud which has been shown to coexpress vimentin and Pax2 under some circumstances.[20] Further studies are required to fully characterize the different cell population(s) that migrate into the scaffold and how these findings will relate to future kidney regeneration strategies. These results demonstrate the intrinsic capacity of decellularized kidney sections to potentiate cell–cell and cell–ECM interactions to facilitate cell-specific infiltration and begin to establish a catalog of cells that do well in decellularized tissue of a given age. These findings also establish a basis for renal recellularization and may provide a paradigm shift in how decellularized tissues of different ages are recellularized.

Taken together, these data establish foundations for *in vitro* renal tissue engineering with decellularized kidney scaffolds, begin to address the impact of age in both decellularization and recellularization, and form the basis for methods that may be necessary for eventual *in vivo* transplantation for patients in different age groups. More extensive recellularization experiments with a range of cell populations will be necessary to assess the full potential of these scaffolds and understand the usefulness of different cell lineages for recellularization strategies. In addition, future investigations will need to focus on the potential retention of major histocompatibility complex (MHC) class I and II antigens and other cell debris that may have the potential to elicit an immune response from the host. Findings from this study serve as initial steps toward the development of future engineered renal constructs and will set the stage for preclinical studies in nonhuman primates.[18,32]

Acknowledgments

The authors thank the members of the animal care staff at the CNPRC and Dr. Kent Leach for use of the Instron mechanical testing device. These studies were supported by the California Institute for Regenerative Medicine (CIRM) Comprehensive grant (no. RC1-00144), the Center of Excellence in Translational Human Stem Cell Research (grant no. HL085036), the UC Davis Stem Cell Training Program (CIRM no. T1-00006), the UC Davis Clinical and Translational Science Center (CTSC) T32 Pre-Doctoral Clinical Research Training Program (5TL1RR024145), and the CNPRC base operating grant (no. RR00169).

Disclosure Statement

No competing financial interests exist.

References

1. National transplant statistics: Kidney transplants 2008, Scientific Registry for Transplant Recipients. Available at www.ustransplant.org/csr/current/nats.aspx. Last accessed September 6, 2009.
2. Gilbert, T.W., Sellaro, T.L., and Badylak, S.F. Decellularization of tissues and organs. Biomaterials **27,** 3675, 2006.
3. Kolker, A.R., Brown, D.J., Redstone, J.S., Scarpinato, V.M., and Wallack, M.K. Multilayer reconstruction of abdominal wall defects with acellular dermal allograft (AlloDerm) and component separation. Ann Plast Surg **55,** 36, 2005.
4. Wainwright, D.J. Use of an acellular allograft dermal matrix (AlloDerm) in the management of full-thickness burns. Burns **21,** 243, 1995.
5. Ferguson, R.E., Jr., and Pu, L.L. Repair of the abdominal donor-site fascial defect with small intestinal submucosa (Sugrisis) after TRAM flap breast reconstruction. Ann Plast Surg **58,** 95, 2007.
6. Tavakkol, Z., Gelehrter, S., Goldberg, C.S., Bove, E.L., Devancy, E.J., and Ohye, R.G. Superior durability of SynerGraft pulmonary allografts compared with standard cryopreserved allografts. Ann Thorac Surg **80,** 1610, 2005.
7. Lichtenberg, A., Tudorache, I., Cebotari, S., Suprunov, M., Tudorache, G., Goerler, H., Park, J.K., Hilfiker-Kleiner, D., Ringes-Lichtenberg, S., Karck, M., Brandes, G., Hilfiker, A., and Haverich, A. Preclinical testing of tissue-engineered heart valves re-endothelialized under simulated physiological conditions. Circulation **114,** I-559, 2006.
8. el-Kassaby, A., AbouShwareb, T., and Atala, A. Randomized comparative study between buccal mucosal and acellular bladder matrix grafts in complex anterior urethral strictures. J Urol **179,** 1432, 2008.
9. Ott, H.C., Matthiesen, T.S., Goh, S.K., Black, L.D., Kren, S.M., Netoff, T.I., and Taylor, D.A. Perfusion-decellularized matrix: using nature's platform to engineer a bioartificial heart. Nature **14,** 213, 2008.
10. Harrison, R.D., and Gratzer, P.F. Effect of extraction protocols and epidermal growth factor on the cellular repopulation of decellularized anterior cruciate ligament allografts. J Biomed Mater Res A **75,** 841, 2005.
11. Karabekmez, F.E., Duymaz, A., and Moran, S.L. Early clinical outcomes with the use of decellularized nerve allograft for repair of sensory defects within the hand. Hand **4,** 245, 2009.
12. Wilshaw, S.P., Kearney, J.N., Fisher, J., and Ingham, E. Production of an acellular amniotic membrane matrix for use in tissue engineering. Tissue Eng **12,** 2117, 2006.
13. Xu, C.C., Chan, R.W., and Tirunagari, N. A biodegradable, acellular xenogeneic scaffold for regeneration of the vocal fold lamina propria. Tissue Eng **13,** 551, 2007.
14. Bhrany, A.D., Beckstead, B.L., Lang, T.C., Farwell, D.G., Giachelli, C.M., and Ratner, B.D. Development of an esophagus acellular matrix tissue scaffold. Tissue Eng **12,** 319, 2006.
15. Macchiarini, P., Jungebluth, P., Go, T., Asnaghi, M.A., Rees, L.E., Cogan, T.A., Dodson, A., Martorell, J., Bellini, S., Parnigotto, P.P., Dickinson, S.C., Hollander, A.P., Mantero, S., Conconi, M.T., and Birchall, M.A. Clinical transplantation of a tissue-engineered airway. Lancet **372,** 2023, 2008.
16. Conconi, M.T., De Coppi, P., Di Liddo, R., Vigolo, S., Zanon, G.F., Parnigotto, P.P., and Nussdorfer, G.G. Tracheal matrices, obtained by a detergent-enzymatic method, support *in vitro* the adhesion of chondrocytes and tracheal epithelial cells. Transpl Int **18,** 727, 2005.
17. Linke, K., Schanz, J., Hansmann, J., Walles, T., Brunner, H., and Mertsching, H. Engineered liver-like tissue on a capillarized matrix for applied research. Tissue Eng **12,** 2699, 2007.
18. Tarantal, A.F., Han, V.K., Cochrum, K.C., Mok, A., daSilva, M., and Matsell, D.G. Fetal rhesus monkey model of obstructive renal dysplasia. Kidney Int **59,** 446, 2001.
19. Leapley, A.C., Lee, C.C., Batchelder, C.A., Yoder, M.C., Matsell, D.G., and Tarantal, A.F. Characterization and culture of fetal rhesus monkey renal cortical cells. Pediatr Res **66,** 448, 2009.
20. Batchelder, C.A., Lee, C.C., Matsell, D.G., Yoder, M.C., and Tarantal, A.F. Renal ontogeny in the rhesus monkey (*Macaca*

mulatta) and directed differentiation of human embryonic stem cells towards kidney precursors. Differentiation **78,** 45, 2009.
21. National Kidney Foundation: Kidney disease. Available at www.kidney.org/kidneyDisease/. Last accessed September 6, 2009.
22. Benfield, M.R., McDonald, R., Sullivan, E.K., Stablein, D.M., and Tejani, A. The 1997 Annual Renal Transplantation in Children Report of the North American Pediatric Renal Transplant Cooperative Study (NAPRTCS). Pediatr Transplant **3,** 152, 1999.
23. Joraku, A., Stern, K.A., Atala, A., and Yoo, J.J. *In vitro* generation of three-dimensional renal structures. Methods **47,** 129, 2009.
24. Rosines, E., Sampogna, R.V., Johkura, K., Vaughn, D.A., Choi, Y., Sakurai, H., Shah, M.M., and Nigam, S.K. Staged *in vitro* reconstruction and implantation of engineered rat kidney tissue. Proc Natl Acad Sci USA **104,** 20938, 2007.
25. Horster, M., Huber, S., Tschop, J., Dittrich, G., and Braun, G. Epithelial nephrogenesis. Eur J Physiol **434,** 647, 1997.
26. Sariola, H. Nephron induction revisited: from caps to condensates. Curr Opin Nephrol Hypertens **11,** 17, 2002.
27. Vize, P.D., Woolf, A.S., and Bard, J.B.L. The Kidney. Orlando: Academic Press, 2003.
28. Kanwar, Y.S., Wada, J., Lin, S., Danesh, F.R., Chugh, S.S., Yang, Q., Banerjee, T., and Lomasney, J.W. Update of extracellular matrix, its receptors, and cell adhesion molecules in mammalian nephrogenesis. Am J Renal Physiol **286,** F202, 2004.
29. Cartmell, J.S., and Dunn, M.G. Effect of chemical treatments on tendon cellularity and mechanical properties. J Biomed Mater Res **49,** 134, 2000.
30. Woods, T., and Gratzer, P.F. Effectiveness of three extraction techniques in the development of a decellularized bone-anterior cruciate ligament (ACL)-bone graft. Biomaterials **26,** 7339, 2005.
31. Lee, C.I., Goldstein, O., Han, V.K., and Tarantal, A.F. IGF-II and IGF binding protein (IGFBP-1, IGFBP-3) gene expression in fetal rhesus monkey tissues during the second and third trimesters. Pediatr Res **49,** 379, 2001.
32. Matsell, D.G., Mok, A., and Tarantal, A.F. Altered primate glomerular development due to *in utero* urinary tract obstruction. Kidney Int **61,** 1263, 2002.
33. Tarantal, A.F. Ultrasound imaging in rhesus (*Macaca mulatta*) and long-tailed (*Macaca fascicularis*) macaques: Reproductive and research applications. In: Wolfe-Cooke, S., ed., The Laboratory Primate. London, UK: Elsevier Academic Press, 2005, Chapter 20.
34. Saxen, L. Organogenesis of the Kidney. Cambridge: Cambridge University Press, 1987.
35. Saltzman, W.M. Tissue Engineering. Oxford: Oxford University Press, 2004.
36. Gratzer, P.F., Harrison, R.D., and Woods, T. Matrix alteration and not residual sodium dodecyl sulfate cytotoxicity affects the cellular repopulation of a decellularized matrix. Tissue Eng **12,** 2975, 2006.
37. Bhrany, A.D., Beckstead, B.L, Lang, T.C., Farwell, D.G., Giachelli, C.M., and Ratner, B.D. Development of an esophagus acellular matrix tissue scaffold. Tissue Eng **12,** 319, 2006.
38. Brown, A.L., Brook-Allred, T.T., Waddell, J.E., White, J., Werkmeister, J.A., Ramshaw, J.A., Bagli, D.J., and Woodhouse, K.A. Bladder acellular matrix as a substrate for studying *in vitro* bladder smooth muscle-urothelial cell interactions. Biomaterials **26,** 529, 2005.
39. Cartmell, J.S., and Dunn, M.G. Development of cell-seeded patellar tendon allografts for anterior cruciate ligaments reconstruction. Tissue Eng **10,** 1065, 2004.

Address correspondence to:
Alice F. Tarantal, Ph.D.
California National Primate Research Center
University of California
Pedrick and Hutchison Roads
Davis, CA 95616-8542

E-mail: aftarantal@primate.ucdavis.edu

Received: September 07, 2009
Accepted: February 15, 2010
Online Publication Date: March 24, 2010